Materials & Design 262 (2026) 115489

Contents lists available at ScienceDirect

Materials & Design

journal homepage: www.elsevier.com/locate/matdes

Quantum chemical insights into molecular interactions within asphalt systems

Guannan Li [a], Mengyuan He [b], Changjiang Dai [c], Liang He [c,*], Tianling Wang [d,*], Xin Liu [c]

[a] School of Traffic and Transportation, Chongqing Jiaotong University, Chongqing 400074, China
[b] School of Materials Science and Engineering, Chongqing Jiaotong University, Chongqing 400074, China
[c] School of Civil Engineering, Chongqing Jiaotong University, Chongqing 400074, China
[d] Institute of Highway Engineering, RWTH Aachen University, Aachen 52074, Germany

ARTICLE INFO

Keywords:
Quantum chemical calculations
Molecular aggregation
Asphalt components
π–π stacking interactions

ABSTRACT

Molecular aggregation significantly impacts the stability, rheology, and durability of asphalt binders. While previous research has mainly focused on asphaltenes, the quantum-scale mechanisms of aggregation for all asphalt components remain unclear. This study uses quantum chemical calculations on 50 asphalt molecules to analyze surface electrostatic potential, π-electron properties, LOLIPOP index, and weak interaction energies to identify favorable aggregation configurations. The findings reveal that π-π interactions drive asphaltene aggregation, resins act as modifiers, aromatics enhance solubility and dispersibility, and saturated hydrocarbons create steric hindrance. Additionally, the length of polycyclic aromatic hydrocarbons and alkyl chains play a critical role in determining intermolecular distance and polarity. SARA fractionation and^1H NMR analysis of four binders show that TH asphalt, rich in π-electron-dense components with long side chains, stabilizes the microstructure, resulting in optimal rheological properties. AFM imaging reveals a honeycomb structure primarily formed by asphaltene-driven aggregation. In summary, this computational-experimental framework elucidates the molecular origins of asphalt aggregation and the distinct roles of SARA components, establishes a clear composition-performance relationship, and provides mechanistic guidance for designing durable asphalt.

1. Introduction

Asphalt is a highly complex, multicomponent material composed of saturates, aromatics, resins, and asphaltenes. The interplay among these molecular constituents governs asphalt's structural stability, rheological behavior, and long-term performance in civil and industrial applications. Among them, asphaltenes are known to be the primary aggregating species, contributing to phenomena such as flocculation, aging, and phase separation.

Asphaltenes fragments have a structure of 7–9 condensed aromatic rings with heteroatoms, which makes them highly polarizable and have a strong tendency to self-aggregate [1]. Malinowski et al. have also pointed out that asphaltenes in asphalt have the highest chemical reactivity and electron-donating and accepting capabilities [2]. Microscopically, asphaltenes aggregation is considered to be caused by pi-pi interactions, polar induction, and electrostatic attraction between molecular sheets [3]. Wang et al. used non-covalent interaction (NCI) analysis to reveal the structure-aggregation relationship of asphaltenes dimers and believed that π-π stacking interactions are the main driving force for asphaltenes aggregation [4]. Murgich et al. investigated the aggregation behavior of asphaltenes and resins through molecular dynamics [5]. The above studies mainly focus on the aggregation of asphaltenes. Even though asphaltenes exhibit the strongest aggregation properties in asphalt, other molecules also have a significant impact on the aggregation process [6]. However, recent studies suggest that non-asphaltene components-particularly resins and aromatics—may also influence molecular aggregation through solvation, interfacial modulation, or steric effects. Despite their potential impact, the specific roles of these secondary species in aggregation remain poorly understood at the molecular level.

Understanding the nature of intermolecular interactions in asphalt is particularly important in the context of its colloidal behavior [7]. Asphalt is widely regarded as a colloidal system in which asphaltenes serve as the dispersed phase, stabilized by resins within an aromatic-rich medium [8–10]. The modified yen model refines this picture by proposing a hierarchical aggregation process, where asphaltene molecules

* Corresponding authors.
E-mail addresses: lianghe@cqjtu.edu.cn (L. He), tianling.wang@rwth-aachen.de (T. Wang).

https://doi.org/10.1016/j.matdes.2026.115489
Received 13 November 2025; Received in revised form 31 December 2025; Accepted 12 January 2026
Available online 13 January 2026

self-associate into nanoaggregates (~7 molecules), which can further form clusters and flocs depending on concentration, temperature, and solvent environment [1,11]. These multi-scale aggregates govern asphalt's sol–gel transition and have a direct impact on its macroscopic rheology. Changes in SARA composition, such as excess saturates or depletion of aromatics, can disrupt this structural equilibrium.

Advancements in quantum chemical simulations have enabled more precise exploration of non-covalent interactions among asphalt molecules [12]. Compared with empirical or classical force field methods, quantum-level approaches allow for accurate evaluation of electron distribution, π–π stacking, electrostatic potentials, and energy surfaces associated with molecular interactions.

Previous studies have applied quantum chemical methods to probe the molecular structure and aging behavior of asphalt [13]. Ruiz-Morales *et al.* investigated various aromatic ring assemblies via HOMO–LUMO gap analysis and showed that alkyl chains and heteroatoms have negligible effects on the gap, with asphaltenes typically containing 5–10 fused aromatic rings arranged in *peri*-condensed structures [14]. Pan *et al.* identified ketones and sulfoxides as the main oxidation products during asphalt aging [15], while Mousavi *et al.* found that α-tocopherol in bio-asphalt undergoes preferential oxidation, thereby delaying asphaltene degradation [16]. Hu *et al.* calculated free energy changes in asphaltene oxidation and noted that aromatization has the lowest energy barrier among competing pathways [17]. Liu *et al.* studied 12 model molecules to identify reactive sites and proposed an aging model and anti-aging strategies [18], furthermore, she also integrated WAXS/SAXS, quantum chemistry, and molecular dynamics to elucidate the hierarchical molecular-micellar-colloidal structure of asphalt, confirming that π–π stacking, electrostatic interactions, and steric effects collectively govern multiscale aggregation and rheological behavior [19]. Tang *et al.* analyzed interaction energies between asphaltenes and resins during aging and regeneration [20]. Li *et al.* demonstrated that chemical modification using diisocyanate additives involves covalent bonding with active sites on asphaltenes and resins [21]. Malinowski *et al.* emphasized the high reactivity and oxidative susceptibility of asphaltenes under atmospheric exposure [22]. Although still underutilized in asphalt research, quantum chemical approaches provide a rigorous framework for elucidating intermolecular interactions, thermodynamic behavior, and reactivity in complex multicomponent systems, thus offering essential molecular-level insights to support experimental observations and guide material design.

Based on the above research and drawing on our team's long-term research in asphalt molecular modeling [19,23,24], this study employed quantum chemical methods to analyze 50 representative asphalt molecules. Surface electrostatic potential distributions and extremum points were calculated to assess polarity and interaction tendencies. Delocalized π electrons structures and LOLIPOP indices were examined to reveal the aggregation behavior of typical molecules and the influence of various asphalt component molecules on aggregation. Simultaneously, weak interaction analysis was performed to determine the optimal intermolecular distance for forming stable aggregates. The intrinsic characteristics of asphalt molecule self-association and the relationship between molecular structure and aggregation behavior were revealed. Through experiments, a clear composition-performance relationship was explained and established. These studies provide mechanistic guidance for the design of durable asphalt.

2. Methodology

2.1. Computational methods

The fifty representative asphalt molecules analyzed in this study were developed by our research group through an integrated experimental-theoretical framework combining SARA fractionation, NMR spectroscopy, elemental analysis, and quantum chemical optimization. The molecular library was designed to capture the compositional and structural diversity of the four SARA fractions. Specifically, asphaltenes (500–1000 amu) consist of 5–10 fused aromatic rings with *peri*-condensed polyaromatic structures; resins are polar aromatics containing heteroatoms (O, N, S) and exhibit moderate dipole moments; aromatics are low-polarity mono- or polyaromatic hydrocarbons with short alkyl chains; and saturates are long-chain alkanes and cycloalkanes representing the non-polar medium. The representativeness of this molecular ensemble was validated by comparing dipole-moment/molecular-mass distributions and HOMO-LUMO gap statistics with experimental data, ensuring its reliability for quantum-scale analysis [24,25].

All quantum chemical calculations in this study were conducted using the GAUSSIAN 16 software package [26]. Based on asphalt molecular models previously developed by our research group [25]-designed to capture the polarity differences among the four SARA fractions-the computational workflow followed the procedure illustrated in Fig. 1. First, geometry optimization was performed using the B3LYP27/def2-SVP level of theory. Single-point energy calculations were then carried out at the B3LYP27/def2-TZVP level to eliminate imaginary frequencies [27]. Dipole moment-related properties and surface electrostatic potential distributions were calculated at the B3LYP/6–31 + G(d,p) level for 50 asphalt molecules. Based on these results, delocalized π-electron densities and LOLIPOP indices were analyzed to assess aggregation tendencies. Finally, weak intermolecular interaction analyses were performed to determine optimal configurations for stable aggregate formation. All wavefunction analyses were carried out using the Multiwfn 3.8 program [28,29], while visualization and post-processing were completed with VMD 1.9.4.[30].

To identify electrostatic potential (ESP) extrema on the molecular surface, Multiwfn employs a grid-based method combined with the marching tetrahedra (MT) algorithm [29]. First, a three-dimensional electron density grid is generated by expanding the molecular structure by a certain radius in all directions. Based on this grid, an isosurface corresponding to an electron density of 0.001 a.u. is constructed, where the surface is discretized into a mesh of triangular elements. Surface vertices are refined through interpolation to improve accuracy. Redundant vertices, typically arising from uneven grid density, are eliminated using a distance-based threshold to reduce computational load. ESP values are then evaluated at each retained vertex, and local extrema are determined by comparing each vertex with its neighboring points.

The majority of asphalt components contain polycyclic aromatic hydrocarbon structures, whose aggregation is influenced by π-π stacking interactions. Since π-π interactions are widely recognized as a primary driving force for molecular aggregation in asphalt, the LOLIPOP index, which reflects π-electron delocalization, is employed here to evaluate the asphalt system. The LOLIPOP index is defined as the definite integral of the localized orbital locator for π electrons (LOL-π) at a plane 0.5 Å above the molecular plane, considering only regions where LOL-π $>$ 0.55. The integration is performed within a cylindrical region perpendicular to the molecular plane, with a radius of 1.94 Å, an average derived from the typical carbon–hydrogen distance in benzene, used to assess the π-stacking capacity of aromatic systems Numerous studies have shown that aromatic rings with lower LOLIPOP values exhibit reduced π-electron delocalization and tend to have stronger π–π stacking interactions [31].

Weak interactions refer to non-covalent forces excluding ionic bonds, such as hydrogen bonding and van der Waals forces, which play a crucial role in determining molecular cluster conformations, physical adsorption behavior, and supramolecular assembly. Research on weak interactions generally focuses on three aspects: interaction energy, structural responses under weak interactions, and the fundamental nature of such interactions. The weak interaction energy scanning was performed based on prior analyses of surface electrostatic potentials and frontier molecular orbitals, and revealed distinct energy extrema for the examined molecular pairs, indicating that, in this system, the corresponding molecular configurations adopt the most stable structures at

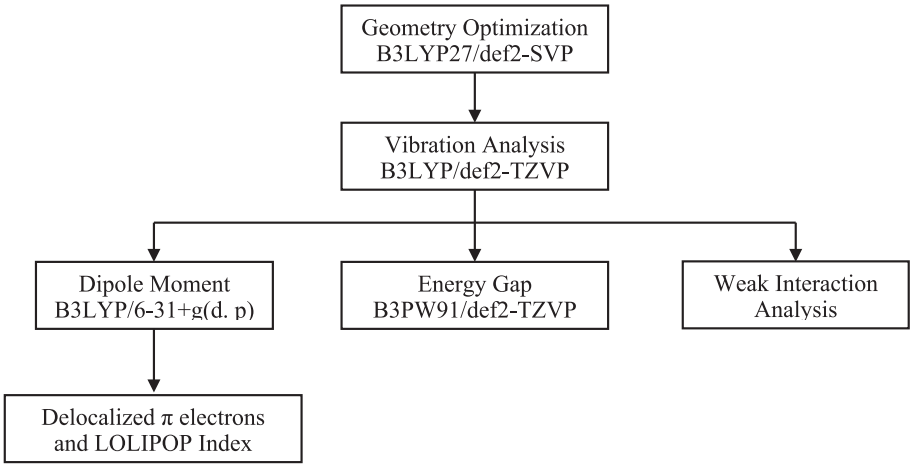

Fig. 1. Quantum Chemistry Theoretical Methods and Basis Set Selection.

these distances, which also represent the optimal separation required for the formation of stable intermolecular aggregates. In this study, weak interaction analysis was conducted by scanning the interaction energy across varying intermolecular distances. The weak interaction energy minima were used to identify optimal binding configurations between different asphalt molecular components, thereby revealing how intermolecular distances influence potential aggregation behavior within the asphalt matrix. Representative molecules of asphaltenes, resins, and aromatics were first screened based on their surface electrostatic potentials to identify likely candidates for weak interaction. Initial dimer configurations were constructed and adjusted using GaussView, with scanning positions, step size, and total steps defined using the Dimer-Scan software [32]. Multi-step scanning input files were generated via Molclus 1.9.9.9 [33], and quantum chemical calculations were then carried out in Gaussian to obtain interaction energies at each scan point, The potential energy surface (PES) scanning method used for weak interaction analysis is illustrated in Fig. 2.

2.2. Experiment methods

Four asphalt binders, denoted as LH, TH, MM, and QL, were selected to represent distinct compositional and colloidal characteristics. The selection was based on SARA fractionation and^1H NMR analyses from previous experimental data. TH asphalt contains the highest proportions of asphaltenes and saturates, resulting in a high colloidal instability index (CII) and classification as a sol–gel type asphalt. LH asphalt, with lower asphaltene and higher aromatic contents, represents a sol-type asphalt with good colloidal dispersion stability. MM asphalt shows intermediate composition and rheological properties between sol and sol–gel types, while QL asphalt serves as a conventional base binder with balanced SARA composition and moderate CII value. These four binders were chosen to ensure representative coverage of different compositional and colloidal states of asphalt.

Additionally, we included a Dynamic Shear Rheometer (DSR) frequency sweep test, with a frequency range from 0.01 to 10 rad/s and a temperature range from 4℃ to 70℃, with intervals of 6℃ and a conditioning time of 900 s. Using the William-Landel-Ferry (WLF) equation from the time–temperature superposition principle, we shifted the frequency sweep results (with 25 °C as the reference temperature), obtaining the master curves for storage modulus and loss modulus of the four typical asphalt samples[24].

Atomic Force Microscopy (AFM) was used to scan the microscopic morphology of LH, TH, MM, and QL asphalts. The AFM analysis was conducted to visualize the surface microstructures of different asphalts and to examine the correspondence between molecular aggregation characteristics and the formation of bee-like domains related to asphaltene content and SARA composition. For AFM sample preparation, the asphalt was heated to soften, and a drop of it was placed on a glass slide. After allowing the sample to rest at room temperature for 24 h, AFM measurements were conducted under ambient laboratory

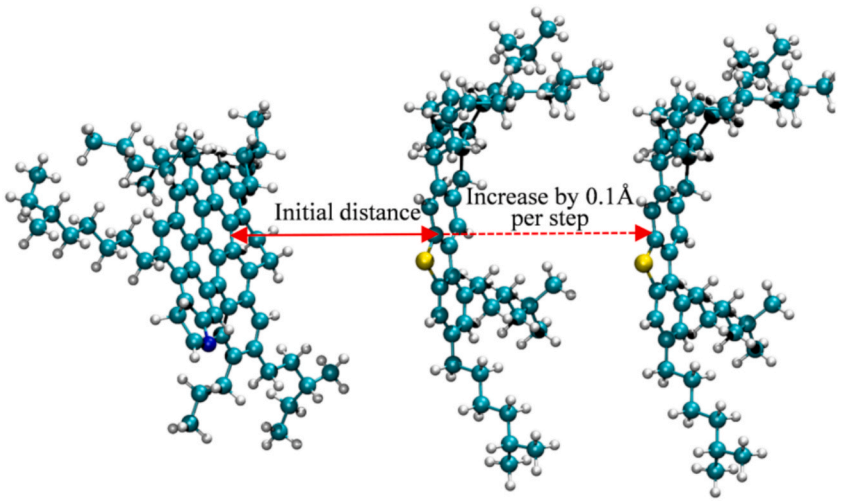

Fig. 2. Schematic diagram of potential energy scanning of As3-R7 molecule.

conditions (approximately 25 °C, 50 % relative humidity). During the AFM testing, the probe was made of silicon material, with a scanning frequency of 0.5 Hz, a tip radius of curvature of 8 nm, a scanning angle of 90 degrees, and a scanning area of 20 × 20 μm^2.

3. Results

3.1. Surface electrostatic potential analysis of asphalt molecules

Negative charge accumulation in asphaltene molecules is primarily concentrated over the parallel planes of polycyclic aromatic regions, resulting in high charge density, as shown in Fig. 3. This suggests that electrostatic interactions between these aromatic cores are repulsive in nature. However, π–π stacking between aggregates is largely governed by dispersion forces; when dispersion dominates over electrostatics, asphalt molecules can still form extended and well-aligned π–π assemblies. The electrostatic potential maps clearly indicate that repulsive forces in polycyclic aromatic regions may hinder ideal face-to-face stacking, implying that parallel-displaced stacking is the more favorable π–π aggregation mode for asphaltenes.

To maintain charge neutrality within the molecular system, regions outside the aromatic cores are typically enriched with positive electrostatic potential. However, these positively charged regions are more spatially diffuse. In particular, areas surrounding alkyl side chains exhibit relatively low positive potential density, indicating that these chains are less likely to participate in intermolecular interactions. Instead, they primarily contribute to steric hindrance, preventing excessive aggregation and thereby enhancing the structural stability of the asphalt molecular system.

Heteroatomic functional groups introduce local perturbations in the electrostatic potential field, suggesting they are key contributors to the strong polarity of asphaltene molecules. For example, in molecule As1, the hydroxyl group gives rise to a local electrostatic potential maximum and minimum of + 51.28 kcal/mol and –25.78 kcal/mol, respectively—features that may render this site chemically reactive. A similar pattern is observed in the pyrrole group of molecule As3, with extrema of + 19.27 kcal/mol and –39.19 kcal/mol. In contrast, thiophene groups appear to exert a weaker influence on surface potential. For instance, the thiophene group in As2 exhibits a potential maximum and minimum of + 15.76 kcal/mol and –16.24 kcal/mol, respectively, while those in As6 are + 17.67 kcal/mol and –16.12 kcal/mol. These results suggest that thiophene rings possess relatively low reactivity and primarily act as electronic extensions of the polycyclic aromatic regions.

Electrostatic potential analysis of resin molecules reveals several key characteristics:

(1) Resins typically possess smaller aromatic domains and shorter alkyl side chains. Their negative electrostatic potential is still primarily localized around the π-electron-rich zones formed by mono- or polycyclic aromatic rings, while the regions surrounding the alkyl chains are generally neutral or exhibit mildly positive potential. This distribution pattern enables resin molecules to readily engage in π–π interactions with other π-rich components in asphalt, facilitating the formation of localized aggregate structures.

(2) The overall electrostatic potential distribution of resins tends to be narrower in range, and is more significantly influenced by heteroatomic functional groups. Due to their compact molecular volume and

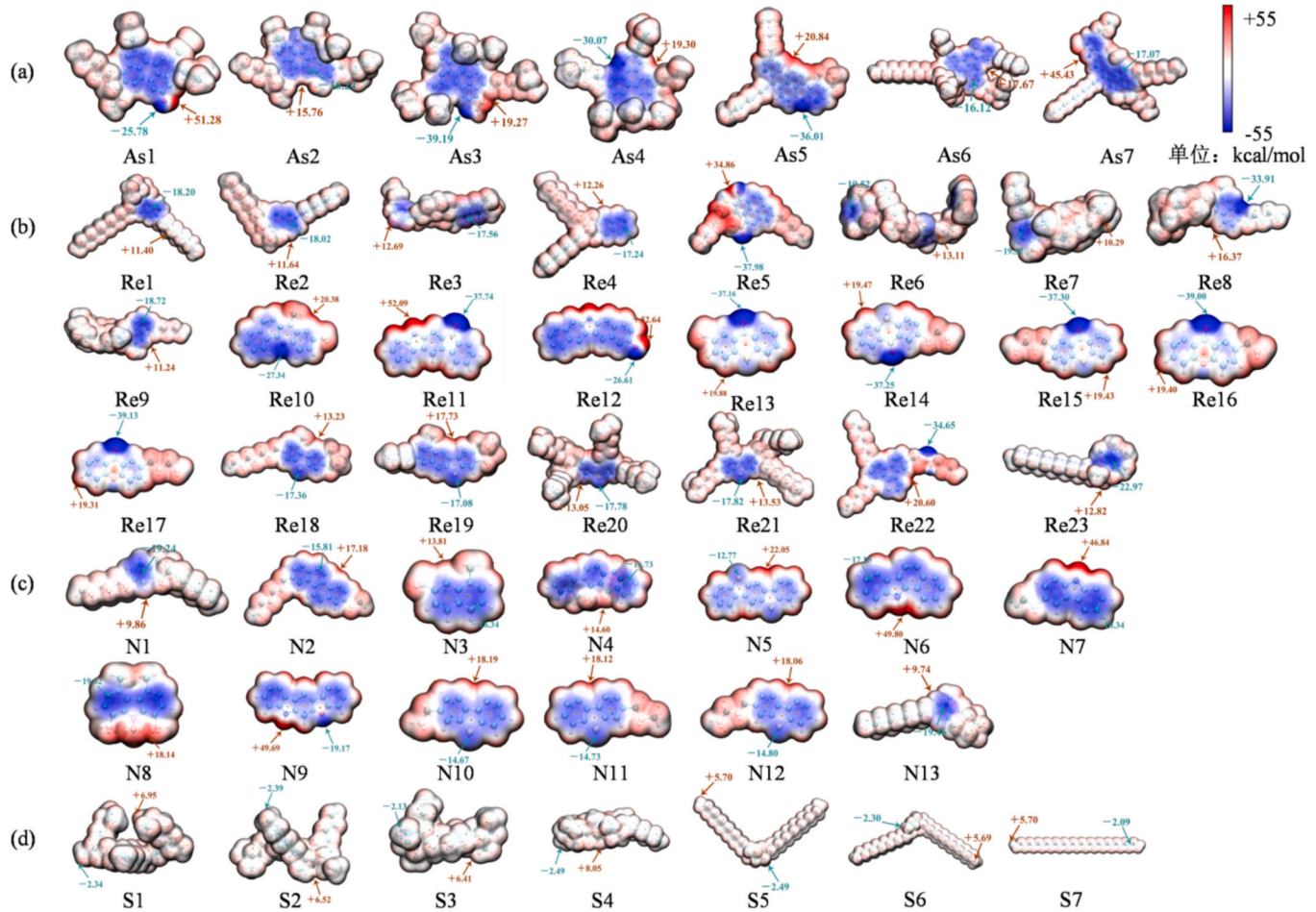

Fig. 3. Distribution of electrostatic potential surface of asphalt molecules. (a) asphaltene molecules,(b) resin molecules,(c) aromatic molecules, and (d)saturate molecules.

short side chains, other structural features in resin molecules are insufficient to effectively shield or delocalize the accumulation of negative potential. As a result, these molecules often display pronounced electrostatic gradients on their surface, with simultaneously concentrated regions of both negative and positive potential. This bipolar electrostatic character allows resins to function as interfacial modulators within the asphalt microstructure, acting as crucial molecular bridges between asphaltenes and aromatics.

(3) Taking resin molecule R9 as a representative example, each side of its central benzene ring is substituted with a hydroxyl functional group, leading to highly localized negative potentials around the hydroxyl groups (with a minimum of –37.98 kcal/mol). In contrast, the cycloalkane region linked to the side chain displays relatively strong positive potential (with a maximum of + 34.86 kcal/mol). Similarly, molecule R15—although lacking side chains—exhibits a strong negative potential minimum near the hydroxyl group (–37.74 kcal/mol), and a symmetrical distribution of highly positive potential at the molecular periphery (maximum of + 52.09 kcal/mol).

Such distinct electrostatic polarization enables resin molecules to participate in aggregation via parallel-displaced or T-shaped π–π stacking configurations, and simultaneously enhances their adsorption affinity toward mineral surfaces. Therefore, the electrostatic potential features of resins play dual roles: influencing the aggregation behavior within the asphalt matrix and regulating interfacial interactions at the asphalt–aggregate boundary.

Aromatics are the smallest and lowest-molecular-weight constituents in asphalt. After polarity-based molecular screening, most aromatic molecules-excluding N6 and N7-exhibit relatively narrow ranges of electrostatic potential, with extrema generally falling between –19.24 kcal/mol and + 18.14 kcal/mol. The aromatic ring remains the primary zone of negative electrostatic potential, yet the overall molecular structure retains its weakly polar nature. Although some aromatic molecules contain heteroatomic functional groups, these groups are typically symmetrically arranged, resulting in low net molecular polarity. These features enable aromatic molecules to maintain good solubility with both asphaltenes and resins, despite their inherently weak polarity.

Saturates, on the other hand, possess larger spatial volumes due to their long alkyl chains or polycyclic alicyclic structures. Their surface electrostatic potentials are nearly neutral, with no significant localized positive or negative charge regions. The overall ESP distribution spans a very narrow range, from –2.49 kcal/mol to + 8.05 kcal/mol, which is markedly lower than that observed for other asphalt fractions. Moreover, saturates lack polar functional groups and are thus intrinsically nonpolar. This absence of polarity implies weak electrostatic interaction potential and low chemical reactivity with other asphalt molecules. The role of saturates in asphalt is predominantly physical: their long, flexible chains interpenetrate or entangle with the alkyl branches of asphaltene and resin molecules, thereby introducing **steric hindrance** that prevents the formation of excessively large aggregates and contributes to the overall stability of the molecular system.

3.2. *Aggregation behavior of asphalt molecules based on delocalized π electrons*

The delocalized π-electron orbitals and LOLIPOP index distributions for representative asphaltene molecules are shown in Figs. 4(a) and (b). The results indicate that regions with high LOL-π values form a continuous ring-like structure, clearly outlining the primary pathways of π-electron delocalization. Given the polycyclic aromatic nature of asphaltenes, the delocalized π-electrons form multiple cyclic domains across the molecular framework. Comparative analysis of the LOLIPOP indices reveals that molecules As3 and As6 exhibit lower LOLIPOP values than As1 and As2, indicating a lower degree of π-electron localization. This suggests that As3 and As6 are more prone to strong π–π interactions and have a higher tendency to form larger asphaltene aggregates.

The delocalized π-electron orbitals and LOLIPOP index distributions for typical resin molecules are illustrated in Figs. 4(c) and (d). The results show that, due to the relatively small number of aromatic rings in resin molecules, the regions of π-electron delocalization are mostly confined to the aromatic planes. Only a limited amount of delocalized π-electron density is observed near heteroatomic functional groups. Comparison of LOLIPOP indices reveals that, with the exception of molecule R9, most resin molecules exhibit higher LOLIPOP values than asphaltenes. This indicates that resins generally have weaker π–π stacking abilities compared to asphaltene molecules. However, R9 stands out due to its dense arrangement of aromatic rings and relatively low LOLIPOP index, suggesting that it may have the potential to form resin-based aggregates under favorable conditions.

The delocalized π-electron orbitals and LOLIPOP index distributions for representative aromatic molecules are shown in Figs. 4(e) and (f). The results indicate that aromatic molecules typically form only 1 to 3 delocalized π-electron rings, primarily localized around the benzene ring regions. While small amounts of delocalized π-electrons are also found near heteroatomic functional groups, the degree of delocalization is relatively low and does not lead to extended ring structures in those areas. According to the LOLIPOP index analysis, aromatic molecules

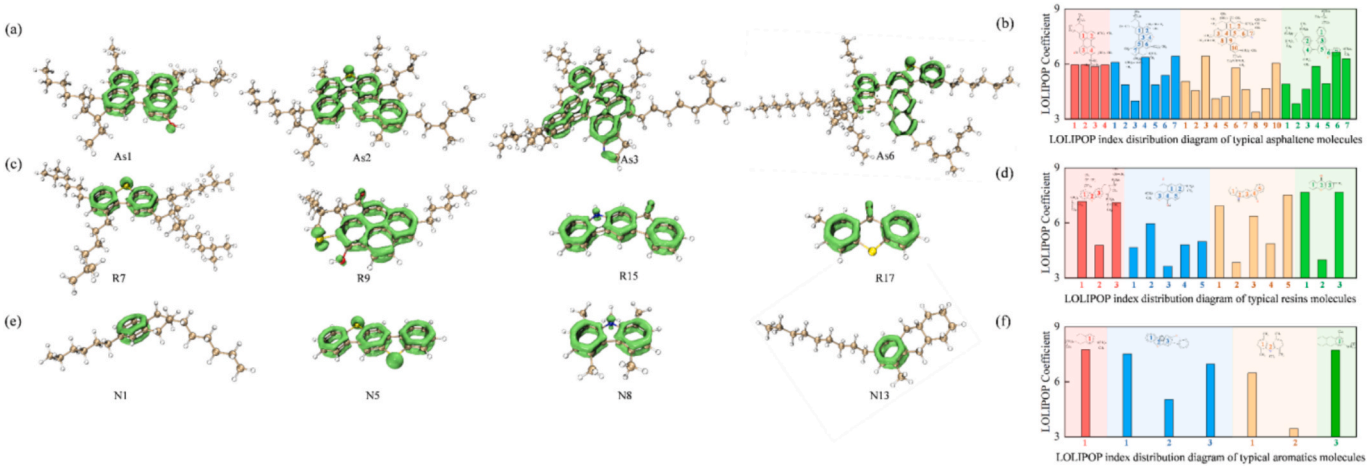

Fig. 4. Schematic diagram of delocalized π orbitals and LOLIPOP index distribution diagram. (a) typical asphaltene molecules, (b) LOLIPOP index distribution diagram of typical asphaltene molecules, (c) typical resin molecules, (d) LOLIPOP index distribution diagram of typical resins molecules, (e) typical aromatic molecules, and (f) LOLIPOP index distribution diagram of typical aromatics molecules.

generally exhibit higher LOLIPOP values than those of asphaltenes and resins. This reflects a greater degree of π-electron localization within individual molecules, which corresponds to a weaker ability to form intermolecular π–π stacked aggregates. Consequently, aromatics are less prone to aggregation through π-interactions compared to asphaltene and resin fractions.

3.3. Analysis of contact characteristics between asphalt molecules

To investigate the optimal intermolecular configurations for aggregation, potential energy surface (PES) scans were conducted between representative asphaltene, resin, and aromatic molecules, as shown in Fig. 5. The results revealed clear energy minima for each molecular pair, indicating the presence of a most stable intermolecular distance where aggregate formation is thermodynamically favorable. The optimal interaction distances were found to be 4.5 Å for asphaltene–asphaltene, 3.7 Å for asphaltene–resin, 4.2 Å for asphaltene–aromatic, 3.6 Å for resin–resin, and 3.4 Å for both resin–aromatic and aromatic–aromatic interactions. These findings show that asphaltenes tend to aggregate at relatively larger distances, whereas aromatic molecules aggregate more closely. Resins and mixed pairs fall in between, suggesting a gradient of aggregation strength and molecular packing across asphalt's SARA components. This trend aligns well with the molecular size, polarity, and π–π stacking potential of each component and provides insight into how different fractions contribute to the microstructural stability of asphalt.

According to classical colloidal theory and the modified Yen model, intermolecular interactions between asphaltene molecules are the primary driving force behind the formation of stable aggregates in asphalt systems. The fundamental chemical structure of asphaltenes can be simplified into four key parameters based on experimental correlations: (I) the number of fused aromatic rings, (II) the presence of polar heteroatomic functional groups, (III) the number of saturated alkyl side chains, and (IV) the average length of these chains. These structural features correspond, respectively, to the carbon-to-hydrogen (C/H) ratio, heteroatom content, and the Hγ and Hβ hydrogen distributions identified via^1H NMR spectroscopy, as illustrated in Fig. 5(k). In the following analysis, the influence of these parameters on intermolecular interactions is systematically examined, alongside variations in molecular dipole moment induced by structural changes.

The effects of structural parameter variations on intermolecular distance, dipole moment, and surface electrostatic potential in asphalt molecules are summarized in Fig. 5(g,h,I,j). The results indicate the following trends:

(1) Changes in the four primary structural components of asphaltene molecules lead to corresponding variations in intermolecular behavior.

(2) When the molecular backbone transitions from perhydrobenzene to a typical polycyclic aromatic hydrocarbon (PAH) structure, the intermolecular distance increases from 3.5 Å to 3.8 Å. Concurrently, the

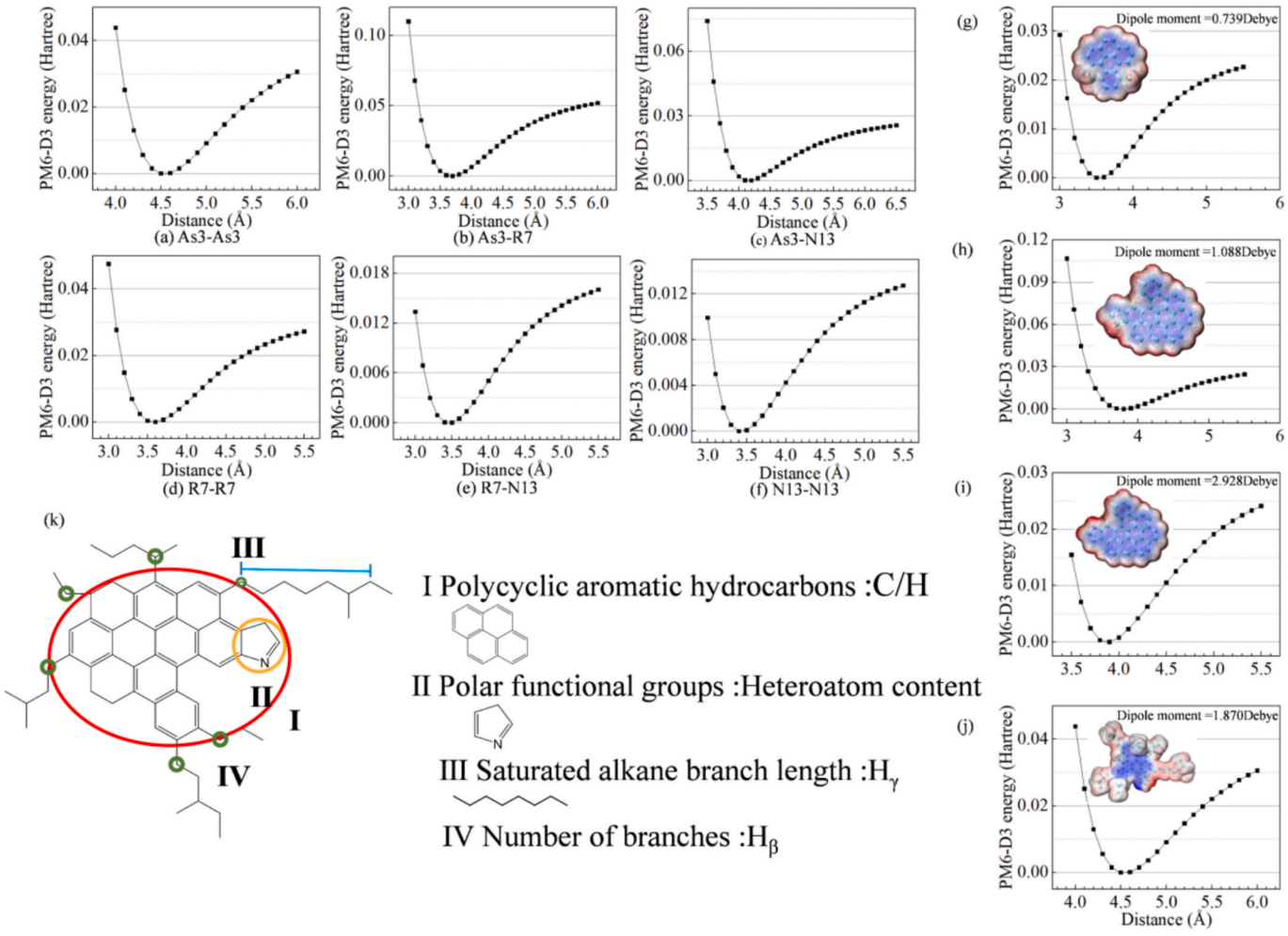

Fig. 5. Interaction Energies and Structural Characteristics of Asphalt molecules and Asphaltenes. (a,b,c,d,e,f)Weak interaction energy variation curves of typical asphalt molecules; Schematic diagram of the variation of asphaltene molecular structure parameters. (g) perhydrobenzene, (h) Main structure of asphaltene polycyclic aromatic hydrocarbons, (i) Polycyclic aromatic hydrocarbon main structure plus nitrogen atom functional group, (j) As3 asphaltene molecules; (k) Effect of chemical composition parameters on molecular spacing of asphaltenes.

dipole moment rises from 0.739 Debye to 1.088 Debye, and electrostatic potential extrema become localized in asymmetrical protruding regions of the molecule.

(3) The introduction of heteroatomic functional groups does not significantly alter the intermolecular distance (increasing only slightly from 3.8 Å to 3.9 Å), but it causes a substantial increase in the dipole moment—from 1.088 Debye to 2.928 Debye. In this case, the region of concentrated electrostatic potential shifts toward the vicinity of the heteroatomic group, with a noticeable increase in charge density.

(4) When multiple saturated alkyl side chains are added to the PAH backbone, the intermolecular distance increases markedly from 3.9 Å to 4.5 Å. This suggests that these side chains introduce spatial hindrance, significantly affecting the aggregation compactness. As the number of side chains increases, the dipole moment decreases from 2.928 Debye to 1.870 Debye, and the location of electrostatic potential extrema shifts accordingly.

Overall, the findings suggest that the number of fused aromatic rings and the presence of alkyl side chains are the dominant factors influencing intermolecular distance in asphaltene aggregation.

3.4. Relationship between asphalt microstructure and rheological properties

In this study, the SARA fractionation results and^1H NMR spectra of the four representative asphalts (LH, TH, MM, and QL) were adopted from our previous work [25]. These data serve as the experimental basis for molecular model construction and parameterization in the present quantum chemical analysis. The SARA composition provided the relative proportions of saturates, aromatics, resins, and asphaltenes, while ^{1}H NMR offered detailed insights into aromaticity, alkyl side-chain distribution, and the presence of heteroatomic functional groups. The key parameters derived from these datasets (C/H ratio, heteroatom content, and H_γ/H_β hydrogen distribution) were directly applied to define the four primary structural variables in the asphaltene molecular models: (I) the number of fused aromatic rings, (II) the type and abundance of polar heteroatomic functional groups, (III) the number of saturated alkyl side chains, and (IV) the average side-chain length. The summarized experimental data are presented in Table 1 and were used as inputs for subsequent computational analyses.

The SARA analysis revealed that TH asphalt contains exceptionally high proportions of asphaltenes and saturates, resulting in a colloidal instability index (CII) far exceeding that of conventional base asphalts. According to the classification of asphalt sol–gel types based on CII values [34], TH asphalt is categorized as a sol–gel type, whereas the other three asphalts fall into the sol-type category. Furthermore, ^{1}H NMR results showed that TH asphalt exhibits an unusually low H_α value and a markedly high H_β value, indicating that its polycyclic aromatic structures contain relatively few side chains or normal alkanes; however, each side chain present is composed of a relatively long, linear alkyl chain.

The DSR frequency sweep results for the four asphalt binders were used to construct master curves based on the time–temperature superposition principle, as shown in Fig. 6(a). Compared with the other three binders, TH asphalt exhibited markedly different rheological characteristics: at low temperatures and high frequencies, both G′ and G″ values were lower, whereas at high temperatures and low frequencies, both G′ and G″ values were significantly higher. This behavior indicates that TH asphalt is softer under low-temperature conditions and stiffer at high temperatures, demonstrating pronounced temperature sensitivity.

Furthermore, rutting and fatigue factors were calculated from the rheological master curves. Using QL asphalt as the reference, the microstructural composition and macroscopic rheological parameters of the four binders were normalized, as illustrated in Fig. 6(b,c,d). TH asphalt showed an exceptionally high proportion of asphaltenes and saturates, with a colloidal instability index (CII) far exceeding that of conventional paving-grade asphalt.

Based on the microstructural composition parameters of asphalt, the molecular distribution of different SARA fractions in TH asphalt was determined and compared with that of QL asphalt, as shown in Fig. 6(e). Distinct differences were observed between the two asphalts. In TH asphalt, asphaltenes were dominated by a higher proportion of As(6) molecules; resins contained greater amounts of R(15) and R(22) molecules; aromatics were enriched in N(2) and N(7) molecules; and saturates exhibited higher proportions of S(5) and S(6) molecules. The asphaltene, resin, and aromatic fractions in TH asphalt all contained a high density of π-electron–rich regions, which favor stronger π–π interactions. At the same time, the presence of longer alkyl side chains hinders the formation of overly compact clusters, thereby contributing to the stability of aggregate structures. In addition, the saturate fraction contains abundant molecules with 1–2 cycloalkane cores and long-chain n-alkanes, which increase the tendency to crystallize and form wax precipitates.

The three-dimensional AFM microtopography of the four typical asphalts is shown in Fig. 6(f,g,h,i). The results reveal that both TH and MM asphalts display distinct bee-like structures; however, the bee-like domains in TH asphalt are noticeably larger in size yet fewer in number compared to those in MM asphalt. In contrast, no such structures were observed in LH or QL asphalt. The origin of bee-like structures has become a research hotspot in recent years, with their formation closely linked to the chemical composition of asphalt. Mainstream interpretations fall into two categories. One school of thought attributes bee-like domains to the stacking of asphaltene fractions, as compositional analyses of these regions have detected aromatic-containing organic compounds—a view supported by researchers such as Masson [35], Hofko [36] and Xing [37] et al。 Another group of scholars believe that the bee-like structure is related to the wax content in the asphalt. When the wax concentration in the asphalt is extremely low, AFM observes a relatively smooth surface of the asphalt, and no honeycomb structure will be observed [38,39].

In the present study, wax content measurements were not conducted; therefore, the possibility of wax crystallization cannot be entirely excluded. However, examination of the microstructural composition data reveals that asphalts displaying bee-like structures possess relatively high asphaltene contents and elevated CII values, suggesting that asphaltene concentration is a key factor in their formation. Moreover, our earlier rheological analysis demonstrated that TH asphalt exhibits excellent performance and favorable temperature susceptibility, whereas increased wax content is generally associated with deteriorated rheological behavior and heightened temperature sensitivity. On this basis, it is unlikely that TH asphalt contains a substantial wax fraction. We therefore infer that asphaltene aggregation, rather than wax crystallization, is the primary contributor to the formation of bee-like structures in this case.

In contrast, the absence of bee-like structures in LH and QL asphalts

Table 1
The chemical composition of 4 typical asphalt.

	As	Re	Ar	Sa	CII	Hα	Hβ	Hγ	C/H
TH	19.8	17.3	33.8	29.1	0.96	3.4	95.1	1.4	8.19
QL	10.4	35.6	42.3	11.8	0.28	13.3	70.5	16.2	8.17
MM	13.2	27.6	44.4	14.7	0.39	20.5	72.7	6.8	8.27
LH	6.5	64.1	12.5	16.9	0.31	9.1	89.6	1.2	8.01

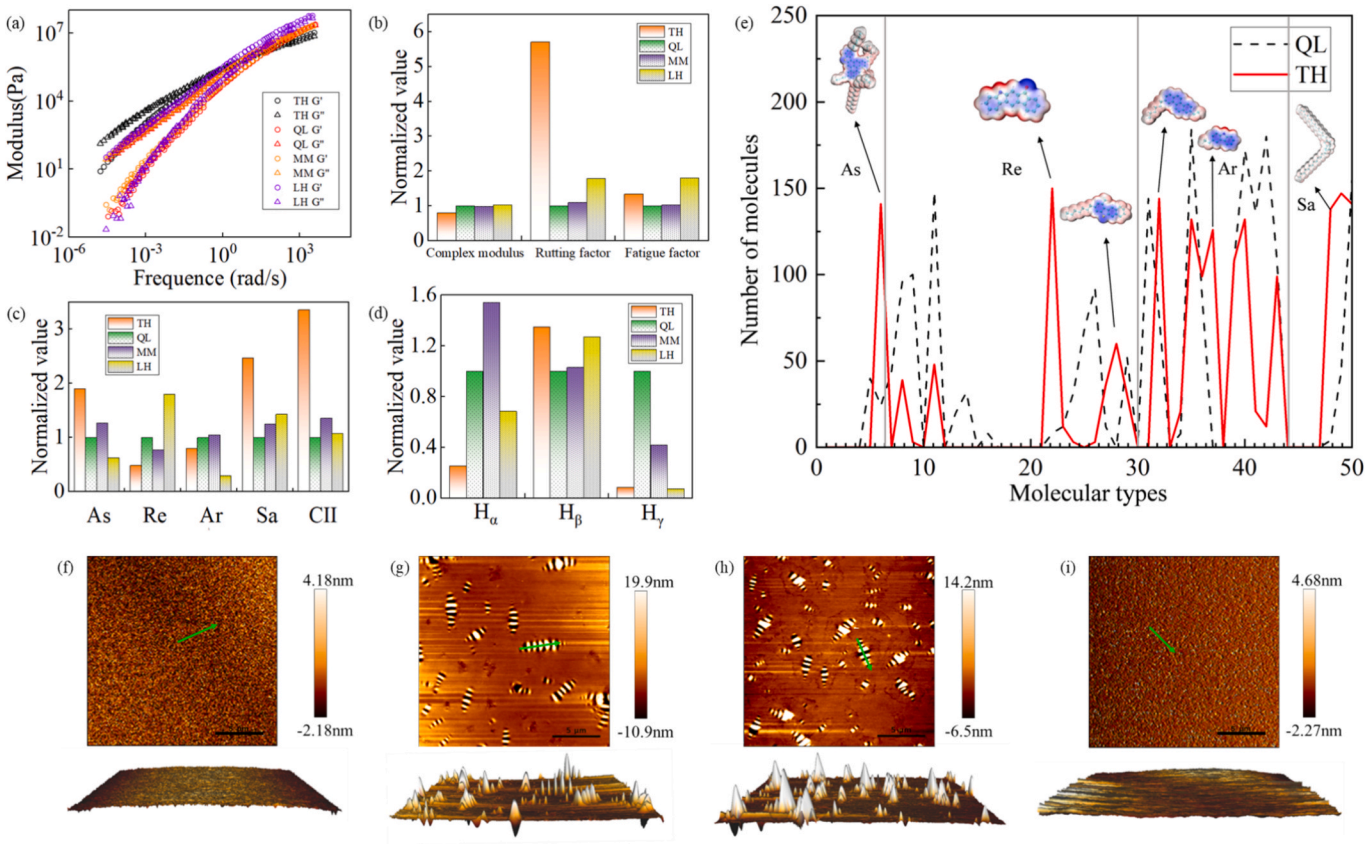

Fig. 6. Analysis of macroscopic properties and molecular microstructure of four asphalt materials. (a) The storage modulus and loss modulus master curves of 4 typical asphalt; (b) The difference of 4 typical asphalt macro performance;(c) The difference of 4 typical asphalt chemical composition;(d) The difference of 4 typical asphalt 1H NMR spectrum;(e) The molecular distribute of TH and QL asphalt; Asphalt AFM scanning asphalt 2D and 3D micromorphology images.(f) LH, (g) TH, (h) MM, (i) QL.

can be attributed to their relatively low asphaltene content, smaller aromatic fractions, and lower colloidal instability indices (CII). Such compositions indicate a weaker tendency for π-π stacking and molecular clustering, resulting in a more homogeneous microstructure with limited phase separation. These microstructural characteristics are consistent with their smoother AFM surfaces and correspond to their lower modulus and weaker temperature sensitivity observed in rheological measurements. Thus, the lack of bee-like morphology reflects a less aggregated, more stable colloidal system dominated by aromatic solvation rather than asphaltene-driven network formation.

4. Conclusion

This study proposes and validates a coupled quantum-chemistry-experimental framework to decode asphalt aggregation, establishing a direct composition-aggregation-property link. By integrating ESP mapping, delocalized π-electron descriptors (including LOLIPOP), weak-interaction energy surface scans, and experiments (SARA,ˆ1H NMR, DSR, AFM).

Asphaltenes show strongly negative ESP on polycyclic aromatic planes, promoting aggregation dominated by π-π interactions and offset stacking. Resins, enriched with heteroatom functionalities, exhibit pronounced polarity gradients and act as interfacial modifiers that bridge asphaltenes and aromatics, stabilizing aggregate structures. Aromatics are weakly polar and highly symmetric, enhancing asphaltene solvation and dispersion, whereas saturates are nearly nonpolar and mainly suppress over-aggregation via steric hindrance.

π-electron topology governs aggregation propensity: highly condensed asphaltenes form extended delocalized π systems with lower LOLIPOP values, indicating stronger π-π association; resins with dense aromatic cores (e.g., R9) can also contribute to aggregation. Energy surface scans define characteristic distance windows for stable aggregates: 4.5 Å (asphaltene-asphaltene), 3.7 Å (asphaltene-resin), and 3.4–4.2 Å (other pairings), reflecting competition between π-π dispersion and electrostatic/steric effects. PAH content and alkyl-chain length most strongly influence interaction distance and dipole moments, thereby controlling aggregate size and stability.

Using TH asphalt as a case, SARA andˆ1H NMR confirm enrichment in π-electron-dense asphaltenes/resins and long-chain aromatics, enabling structural stability while limiting excessive aggregation. DSR indicates a favorable balance between high-temperature stiffness and low-temperature compliance, and AFM reveals honeycomb-like features associated with asphaltene aggregation. Experiments agree with calculations. Overall, we establish an operational microscopic criterion-"π-electron density-steric hindrance-polarity gradient"-that, coupled with rapid SARA andˆ1H NMR, provides mechanistic guidance for stability assessment, quality grading, and formulation optimization. Because crude source, refining history, and modification/rejuvenation can reshape molecular profiles, future work will expand the binder library to validate transferable descriptors and engineering-ready standards.

This work focuses on representative molecular models and intermolecular interactions under idealized conditions, and therefore does not explicitly account for the effects of asphalt aging, chemical modification, or long-term environmental influences. We highlight that evaluation tools such as the LOLIPOP index and weak intermolecular interaction energy analysis, as emerging microscopic descriptors for asphalt systems, hold potential for broader application. Future studies may extend the proposed framework to aged or modified asphalt systems in order to better capture the evolution of molecular interactions

and aggregation behavior under more realistic service conditions.

CRediT authorship contribution statement

Guannan Li: Writing – original draft, Visualization, Software, Methodology, Formal analysis, Conceptualization. **Mengyuan He:** Visualization, Validation, Methodology, Data curation, Conceptualization. **Changjiang Dai:** Writing – review & editing, Validation, Software, Conceptualization. **Liang He:** Supervision, Resources. **Tianling Wang:** Validation, Supervision. **Xin Liu:** Writing – review & editing, Validation.

Declaration of competing interest

The authors declare that they have no known competing financial interests or personal relationships that could have appeared to influence the work reported in this paper.

Acknowledgements

The author would like to give special thanks for financial support from the National Key R&D Program(2024YFB2605303), National Natural Science Foundation of China (52278440), Key R&D Program of Guangxi Province(2024AB08050), CSC Innovative Talent International Cooperation Training Program (CXXM20240031) and the Science and Technology Research Program of Chongqing Municipal Education Commission(KJQN202500715). Thanks to the anonymous reviewers for many comments that have notably helped us improve the manuscript.

Data availability

Data will be made available on request.

References

[1] O.C. Mullins, The modified Yen model, Energy Fuel 24 (2010) 2179–2207.
[2] S. Malinowski, L. Bandura, A. Woszuk, Influence of atmospheric oxygen on the structure and electronic properties of bitumen components–A DFT study, Fuel 325 (2022) 124551.
[3] Z. Wang, The chemistry and physics of petroleum asphaltenes, Asphalt 10 (1996) 26–36.
[4] H. Wang, H. Xu, W. Jia, J. Liu, S. Ren, Revealing the intermolecular interactions of asphaltene dimers by quantum chemical calculations, Energy Fuel 31 (2017) 2488–2495.
[5] J. Murgich, A. Rodríguez, Y. j. e., & fuels. Molecular recognition and molecular mechanics of micelles of some model asphaltenes and resins. 10 (1996) 68–76.
[6] G. Chen, R. Gu, L. Lyu, X. Li, J. Pei, Exploring the unjamming transition of meso-mechanical shear failure behavior in asphalt mixture, Comput. Aided Civ. Inf. Eng. 40 (2025) 4929–4945, https://doi.org/10.1111/mice.70089.
[7] S. Liu, H. Wang, J. Yang, Influence of the Interactions of the Saturate, Aromatic, Resin, and Asphaltene Fractions on the Colloidal Structure of Asphalt: A Study Based on, Mol. Simul. 37 (2025) 04025046, https://doi.org/10.1061/JMCEE7.MTENG-18986.
[8] J.P. Pfeiffer, R.N.J. Saal, Asphaltic Bitumen as Colloid System, J. Phys. Chem. 44 (1940) 139–149, https://doi.org/10.1021/j150398a001.
[9] A. Behnood, M. Modiri Gharehveran, Morphology, Rheology, and Physical Properties of Polymer-Modified Asphalt Binders, Eur. Polym. J. 112 (2019) 766–791, https://doi.org/10.1016/j.eurpolymj.2018.10.049.
[10] G. Rui, et al., Long-tail pollution from asphalt pavements in the context of sustainable urban development, Transp. Res. Part D: Transp. Environ. 150 (2026) 105095, https://doi.org/10.1016/j.trd.2025.105095.
[11] Porto, M. et al. The Structure of Bitumen: Conceptual Models and Experimental Evidences. 15, 905 (2022).
[12] Zhu, J. et al. Selection of Representative Asphaltene Molecules in an Asphalt Molecular Model Based on Quantum Chemistry and Statistical Analysis. 29, 6015 (2024).
[13] M. Hu, S. Ji, M. Li, L. Liu, H. Cheng, Revealing the aging-induced chemical and microstructure evolution of asphalt via AFM-IR and quantum chemistry simulation, Fuel 395 (2025) 135218, https://doi.org/10.1016/j.fuel.2025.135218.
[14] Y. Ruiz-Morales, HOMO-LUMO Gap as an Index of Molecular Size and Structure for Polycyclic Aromatic Hydrocarbons (PAHs) and Asphaltenes: A Theoretical Study. I, Chem. A Eur. J. 106 (2002) 11283–11308.
[15] T. Pan, Y. Lu, S. Lloyd, Quantum-Chemistry Study of Asphalt Oxidative Aging: An XPS-Aided Analysis, Ind. Eng. Chem. Res. 51 (2012) 7957–7966, https://doi.org/10.1021/ie3007215.
[16] J.P.K. Tillett, Axial and transverse Stokes flow past slender axisymmetric bodies, J. Fluid Mech. 44 (1970) 401–417, https://doi.org/10.1017/S0022112070001908.
[17] D. Hu, X. Gu, B. Cui, J. Pei, Q. Zhang, Modeling the Oxidative Aging Kinetics and Pathways of Asphalt: A ReaxFF Molecular Dynamics Study, Energy Fuel 34 (2020) 3601–3613, https://doi.org/10.1021/acs.energyfuels.9b03740.
[18] S. Liu, L. Shan, G. Li, B. Shane Underwood, C. Qi, Molecular-based asphalt oxidation reaction mechanism and aging resistance optimization strategies based on quantum chemistry, Mater. Des. 223 (2022) 111225, https://doi.org/10.1016/j.matdes.2022.111225.
[19] S. Liu, L. Shan, Unraveling the molecular-micellar-colloidal structure of asphalt: From interactions to structural formation, Compos. B Eng. 305 (2025) 112718, https://doi.org/10.1016/j.compositesb.2025.112718.
[20] D. Tang, Y. Zhao, G. Xu, T. Yang, D. Han, Research on the Adsorption Capacity Between Asphaltene and Resin in Asphalt with Different Aging Degree: Experimental Study and Quantum-Mechanical Calculation, J. Clean. Prod. 415 (2023) 137651, https://doi.org/10.1016/j.jclepro.2023.137651.
[21] T. Li, et al., Experimental Investigations and Quantum Chemical Calculations of Methylene Diphenyl Diisocyanate (MDI)-Based Chemically Modified Bitumen and Its Crosslinking Behaviours, Fuel 321 (2022) 124084, https://doi.org/10.1016/j.fuel.2022.124084.
[22] S. Malinowski, L. Bandura, A. Woszuk, Influence of Atmospheric Oxygen on the Structure and Electronic Properties of Bitumen Components: A DFT Study, Fuel 325 (2022) 124551, https://doi.org/10.1016/j.fuel.2022.124551.
[23] L. He, et al., Coarse-grained molecular dynamics reveals rejuvenation behavior in aged asphalt, Comput. Aided Civ. Inf. Eng. (2025), https://doi.org/10.1111/mice.70017.
[24] G. Li, et al., Density, zero shear viscosity and microstructure analysis of asphalt binder using molecular dynamics simulation, Constr. Build. Mater. 345 (2022) 128332, https://doi.org/10.1016/j.conbuildmat.2022.128332.
[25] G. Li, Y. Tan, The Construction and Application of Asphalt Molecular Model Based on Quantum Chemistry Calculation, Fuel 308 (2022) 122037, https://doi.org/10.1016/j.fuel.2021.122037.
[26] Gaussian 16 Rev. C.01 (Wallingford, CT, 2016).
[27] F. Weigend, R. Ahlrichs, Balanced Basis Sets of Split Valence, Triple Zeta Valence and Quadruple Zeta Valence Quality for H to Rn: Design and Assessment of Accuracy, PCCP 7 (2005) 3297–3305, https://doi.org/10.1039/B508541A.
[28] T. Lu, F. Chen, Multiwfn: A Multifunctional Wavefunction Analyzer, J. Comput. Chem. 33 (2012) 580–592, https://doi.org/10.1002/jcc.22885.
[29] T. Lu, A comprehensive electron wavefunction analysis toolbox for chemists, Multiwfn. The Journal of Chemical Physics 161 (2024), https://doi.org/10.1063/5.0216272.
[30] A. Dalke, K. Schulten, VMD: Visual Molecular Dynamics, J. Mol. Graph. 14 (1996) 33–38.
[31] J.F. Gonthier, et al., π-Depletion as a Criterion to Predict π-Stacking Ability, Chem. Commun. 48 (2012) 9239–9241, https://doi.org/10.1039/C2CC33886F.
[32] dimerscan program (Beijing Kein Research Center for Natural Sciences, Beijing, 2023).
[33] Molclus program v. 1.9.9.9 (Beijing Kein Research Center for Natural Sciences, Beijing, 2025).
[34] J. Wang, T. Wang, X. Hou, F. Xiao, Modelling of rheological and chemical properties of asphalt binder considering SARA fraction, Fuel 238 (2019) 320–330, https://doi.org/10.1016/j.fuel.2018.10.126.
[35] V.L. Masson, J. Margeson, S. bundalo-perc., Low-temperature bitumen stiffness and viscous paraffinic nanoand micro-domains by cryogenic AFM and PDM, J. Microsc. 227 (2007) 191–202, https://doi.org/10.1111/j.1365-2818.2007.01796.x.
[36] B. Hofko, et al., Impact of maltene and asphaltene fraction on mechanical behavior and microstructure of bitumen, Mater. Struct. 49 (2016) 829–841, https://doi.org/10.1617/s11527-015-0541-6.
[37] C. Xing, L. Liu, Y. Cui, D. Ding, Analysis of base bitumen chemical composition and aging behaviors via atomic force microscopy-based infrared spectroscopy, Fuel 264 (2020) 116845, https://doi.org/10.1016/j.fuel.2019.116845.
[38] X. Lu, M. Langton, P. Olofsson, P. Redelius, Wax morphology in bitumen, J. Mater. Sci. 40 (2005) 1893–1900, https://doi.org/10.1007/s10853-005-1208-4.
[39] A.T. Pauli, R.W. Grimes, A.G. Beemer, T.F. Turner, J.F. Branthaver, Morphology of asphalts, asphalt fractions and model wax-doped asphalts studied by atomic force microscopy, Int. J. Pavement Eng. 12 (2011) 291–309, https://doi.org/10.1080/10298436.2011.575942.